# High-Spatial-Resolution OH PLIF Visualization in a Cavity-Stabilized Ethylene-Air Turbulent Flame

Clayton M. Geipel[*], Robert D. Rockwell[†], Harsha K. Chelliah[‡]
*University of Virginia, Department of Mechanical and Aerospace Engineering,*
*Charlottesville, Virginia 22904*

Andrew D. Cutler[‡], Christopher A. Spelker[§], Zeid Hashem[§]
*The George Washington University, Department of Mechanical and Aerospace Engineering,*
*Washington, District of Columbia 20052*

*and*

Paul M. Danehy[**]
*NASA Langley Research Center,*
*Hampton, Virginia 23681*

**High-spatial-resolution OH planar laser-induced fluorescence was measured for a premixed ethylene-air turbulent flame in an electrically-heated Mach 2 continuous-flow facility (University of Virginia Supersonic Combustion Facility, Configuration E.) The facility comprised a Mach 2 nozzle, an isolator with flush-wall fuel injectors, a combustor with optical access, and an extender. The flame was anchored at a cavity flameholder with a backward-facing step of height 9 mm. The temperature-insensitive $Q_1(8)$ transition of OH was excited using laser light of wavelength 283.55 nm. A spatial filter was used to create a laser sheet approximately 25 µm thick based on full-width at half maximum (FWHM). Extension tubes increased the magnification of an intensified camera system, achieving in-plane resolution of 40 µm based on a 50% modulation transfer function (MTF). The facility was tested with total temperature 1200 K, total pressure 300 kPa, local fuel/air equivalence ratios of approximately 0.4, and local Mach number of approximately 0.73 in the combustor. A test case with reduced total temperature and another with reduced equivalence ratio were also tested. PLIF images were acquired along a streamwise plane bisecting the cavity flameholder, from the backward facing step to 120 mm downstream of the step. The smallest observed features in the flow had width of approximately 110 µm. Flame surface density was calculated for OH PLIF images.**

## Nomenclature

| | | |
|---|---|---|
| $\eta$ | = | Kolmogorov length scale |
| $f$ | = | f-number |
| $FSD$ | = | flame surface density |
| $H$ | = | cavity height |
| $I$ | = | image intensity |
| $L$ | = | integral length scale |
| $m$ | = | image modulation |
| $M$ | = | image magnification, Mach number |
| $MTF$ | = | modulation transfer function |

[*] Ph.D. Student, Student Member AIAA

[†] Senior Scientist, Member AIAA

[‡] Professor, Department of Mechanical and Aerospace Engineering, Associate Fellow AIAA

[§] Undergraduate Student, Student Member AIAA

[**] Senior Technologist, Associate Fellow AIAA

American Institute of Aeronautics and Astronautics

| $v$ | = | kinematic viscosity |
|---|---|---|
| $P_0$ | = | total pressure |
| $\phi$ | = | fuel/air equivalence ratio |
| $RL$ | = | resolution limit |
| $T_0$ | = | total temperature |
| $u$ | = | root-mean-square velocity |
| $x, y, z$ | = | facility coordinates |
| $x_p, y_p$ | = | pixel coordinates |

## I.    Introduction

PLANAR laser-induced fluorescence (PLIF) is an optical measurement technique in which a thin sheet of laser light excites a chemical species in a fluid flow. The resulting fluorescence is captured by a camera and provides an instantaneous, spatially-resolved, qualitative or quantitative measurement of the concentration of that species. The setup described in this study was used to capture qualitative OH PLIF images at the University of Virginia Supersonic Combustion Facility. This study improves upon the work done by Cantu et al. who previously performed OH PLIF imaging in the same flowpath and facility.[1] Two important changes were made for this study. First, extension tubes were added to the camera lens in order to increase magnification and in-plane resolution. Second, a spatial filter and different laser sheet forming optics were used to create a much thinner laser sheet than used previously.

PLIF systems have been used extensively to image turbulent flames.[2-6] Systems for PLIF and other optical measurement techniques are well-suited for measuring turbulent combustion flows because they are non-intrusive and can be built around existing test facilities. PLIF creates two-dimensional maps indicating the locations of specific chemical species in the flow. Maps of the presence of OH and other combustion products give insight into leading-edge structure of turbulent flames. Maximizing the in-plane spatial resolution and minimizing the thickness of the laser sheet allows examination of the smallest flame structures in the flow. High-spatial-resolution OH PLIF data can be used to validate computational models of turbulent combustion at small length scales.

## II.    Experimental set-up

### A.  Facility

The University of Virginia Supersonic Combustion Facility (UVaSCF)[7,8] is an electrically-heated continuous-flow clean-air facility capable of sustaining a Mach 2 flow with total temperature 1200 K, simulating the enthalpy of a scramjet in Mach 5 flight. The facility configuration used for this study is the so-called "modified Configuration E" described by Rockwell et al.,[9] consisting of a Mach 2 nozzle, followed by an isolator with fuel injectors, the combustor test section, a constant area section, and an extender with an air throttle. Modular design of the facility allows various cavity flameholder designs to be tested in these conditions. Quartz windows allow camera access from two sides for optical techniques such as PLIF. A third side contains a narrow window for introducing a light sheet.

A copper insert was used as the fourth wall for the scramjet combustor. The insert contained a cavity flameholder of height $H = 9$ mm. After the incoming flow is electrically heated, hydrogen is injected into the flow. When the hydrogen flame is established, ethylene enters the flow through flush-wall injectors in the isolator, resulting in a premixed flame that is anchored at the cavity. Figure 1 shows a long-exposure natural luminosity image of combustion in the facility captured with a consumer-grade camera. The image shows a turbulent ethylene-air flame anchored at the backward-facing step of



**Figure 1.  Ethylene-air cavity-stabilized flame at UVaSCF**

the cavity. The coordinate system used in this paper originates in the plane of the rearward-facing step at the downstream projection of the center of the nozzle exit. The $x$-axis is positive in the downstream direction, and the $y$-axis is positive towards the cavity wall.
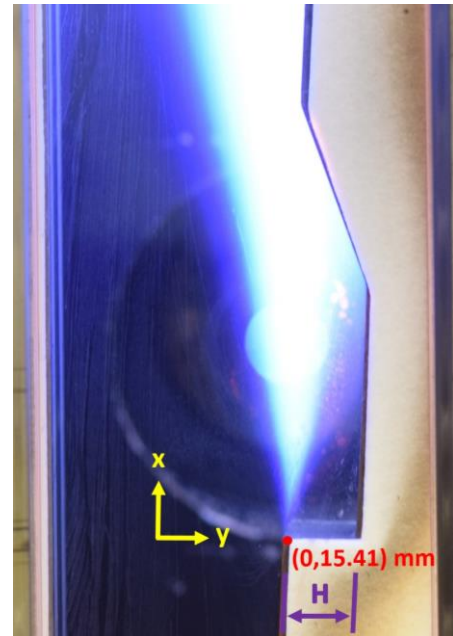
## B. Resolution limit requirement

The size of the smallest eddies in a turbulent flow have is defined by the Kolmogorov length scale.[10] This is the scale at which kinetic energy dissipates via molecular diffusion. A turbulent flow is also described by an integral length scale $L$, which defines the size of the largest eddies in the flow.[11] Previous computational and particle image velocimetry investigations of this flowpath estimated the $L = 5$ mm, root-mean square velocity $u = 50$ m/s, and kinematic viscosity $v = 4$ to 5 m$^2$/s.[12] The Kolmogorov length scale $\eta$ can be estimated[13] using Eq. (1) at 7 to 8 µm.

$$\eta = (v/u)^{3/4} L^{1/4} \tag{1}$$

In his review of turbulent flame structure experiments, Driscoll[14] concludes that eddies at this scale are not strong enough to perturb flame structure. An experiment by Kobayashi et al.[15] suggests that the smallest flame structures are at a scale ten times the Kolmogorov length. Therefore, $10\eta \approx 70$ µm estimates the resolution limit that a PLIF system must achieve to resolve all significant flame structures in the flow.

## C. Beam path

A 1064 nm laser beam pulsed at 20 Hz was generated by Q-switching a SpectraPhysics Nd:YAG laser. This was frequency-doubled to 532 nm and used to pump a Sirah Cobra Stretch dye laser circulating a mixture of Rhodamine 590 and Rhodamine 610 laser dyes. The dye laser output was tuned to 567.10 nm and frequency doubled to 283.55 nm in order to excite the $Q_1(8)$ transition of OH. This transition was used because fluorescence intensity at this wavelength is relatively temperature-independent[1,16] so that variations in signal intensity can be interpreted mainly as OH concentration variations (and not temperature variations). Energy at the output of the dye laser was approximately 15 mJ/pulse.

Figure 2 is a labeled diagram of the beam path. The beam exited the laser cart and passed through a periscope, followed by a pair of cylindrical lenses of focal length 500 mm that focused and then recollimated the beam. All focal lengths in this description are nominal values. A spatial filter (Fig. 3) was placed at the beam focus (location 2 in Fig. 2.) This filter was previously the entrance slit for a spectrometer in which the gap between two steel blades is set by an adjustable knob. The device was modified by putting the blades in backwards so that the blunt ends meet, because the sharp ends were slowly ablated by the laser beam in the original configuration. By narrowing the gap around the beam focus, abnormalities on the edges of the laser sheet were removed.
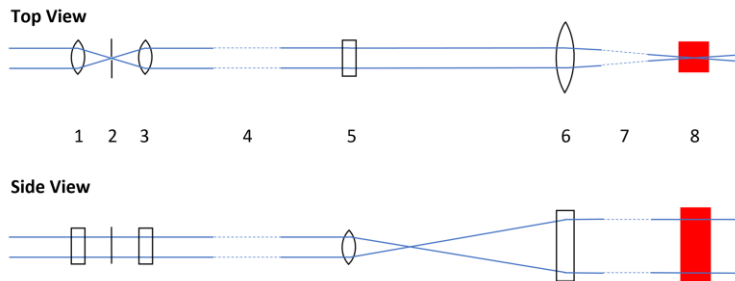


1. 500 mm focal length cylindrical lens
2. Spatial filter
3. 500 mm focal length cylindrical lens
4. Relay mirrors
5. 50 mm focal length cylindrical lens
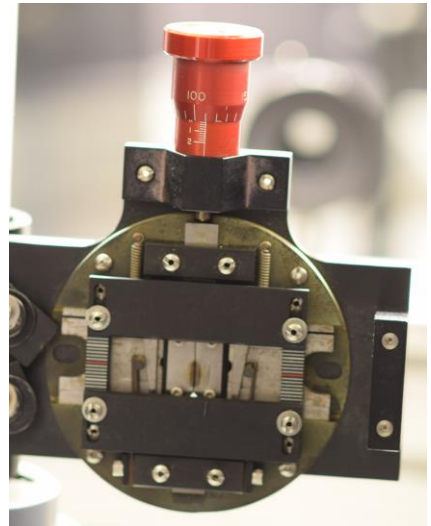6. 300 mm focal length spherical lens
7. planar mirror periscope
8. flame

**Figure 2. Laser sheet optics diagram.** *Not to scale.*



**Figure 3. Spatial filter**

The beam was then routed through a remotely-operated three-axis translation system. Mirrors were set up such that the final laser sheet could be moved in three dimensions. A 50 mm focal length cylindrical lens was used to focus and then expand the beam. A 300 mm focal length spherical lens then collimated the beam in the dimension of this expansion, and focused it in the other dimension to form a laser sheet. Finally, two planar mirrors were used in a periscope configuration to direct the laser sheet into the test section.

## D. Laser sheet profile

The thickness of the laser sheet waist at the test section was measured prior to operating the facility using a 2448 × 2048 pixel, 16-bit CCD beam-profiling camera from Point Grey. The filter in front of the detector was removed to allow the detection of ultraviolet light. The beam was split after the spherical lens and a small percentage was directed into the beam-profiling camera. A single-element fused silica lens of 20 mm focal length was used to directly image the focus on the sensor with 11.3:1 magnification. The lens tube held several neutral density filters designed for ultraviolet light, which were removed individually until a laser sheet profile could be imaged. Decreasing the aperture width of the spatial filter shown in Fig. 3 removed non-Gaussian features from the edges of the sheet, and resulted in a thinner sheet waist.

Figure 4 shows intensity profile across the laser sheet for several spatial filter knob settings. This numerical setting is the width of the spatial filter aperture offset by an arbitrary constant value; the setting is repeatable but it is not an absolute aperture width. The filter was set at 125 μm for OH PLIF. Filter settings smaller than this caused significant ablation of the filter. This setting produced a laser sheet full width at half maximum (FWHM) of approximately 25 μm. The sheet profile at this setting retained some non-Gaussian features.
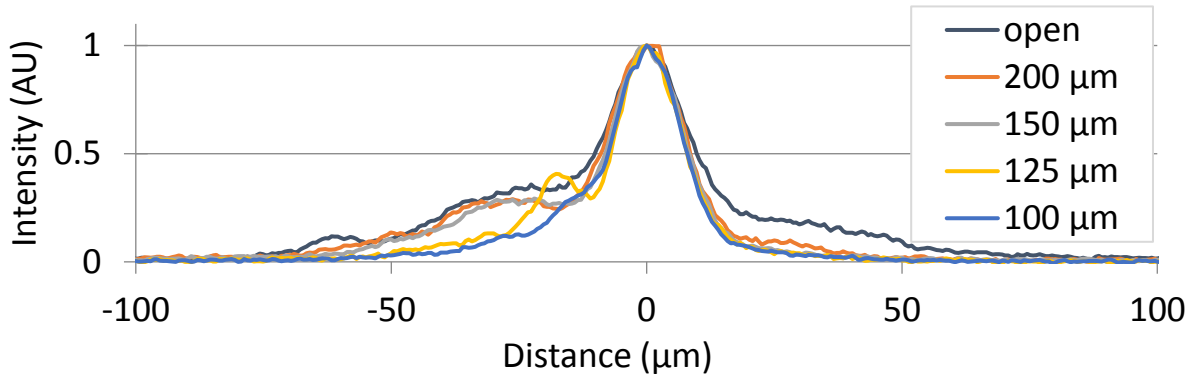
**Figure 4. Laser sheet intensity profiles at various spatial filter settings**

## E. Camera system

OH PLIF images were taken using a PI-Max 4 intensified CCD camera. The camera was mounted on the same three-axis translation system as the laser sheet optics, such that the focus of the laser sheet remained centered in the field of view as the sheet moved. A fourth translation stage allowed the camera to remotely translate closer to and further away from the laser sheet. Using this stage, the camera was remotely focused on the laser sheet during facility operations.

A 100 mm focal length, $f/2.8$ Cerco camera lens was mounted on the camera with extension tubes. The lens contained a Semrock FF02-320/40-30-D bandpass filter, which admits light from 310 to 340 nm; this was used to block laser reflections and other interferences. To characterize the resolution limit of this system, the camera was focused on a USAF-1951 resolution target backlit by an ultraviolet light source (Fig. 5). This glass target presents line pairs of a range of sizes. The lines are alternately transparent and opaque.

**Figure 5. USAF-1951 resolution target.** *Image taken with 76.2 mm extension tube configuration.*

A modulation transfer function *MTF*, defined by Eq. (2) and (3) (Ref. 17), characterized the resolution of the system. Modulation, *m,* is defined as a function of maximum and minimum intensities $I$ in a pair of bright and dark areas. The "image" modulation is recorded at each line pair and compared to a baseline "object" modulation recorded at the large bright square and the surrounding dark area. The resolution limit *RL* of the system is defined as the width of the line pair at which *MTF* = 50%.

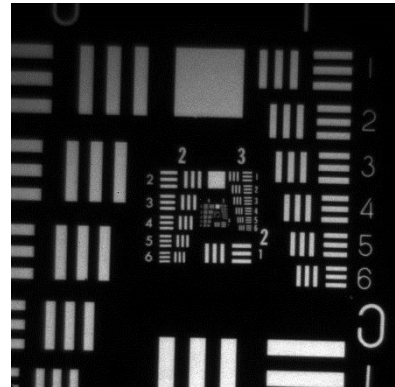$$m = \frac{I_{max} - I_{min}}{I_{max} + I_{min}} \tag{2}$$

$$MTF = \frac{m_{image}}{m_{object}} \qquad (3)$$

Images were taken using three total lengths of extension tubes: 76.2, 152.4, and 203.2 mm. Image magnification values $M$ were recorded for each case and compared with resolution limits. We observed that the product of the resolution limit and the magnification remained approximately constant.. Equation (4) describes this observation; it is valid only for the present camera and lens. Signal intensity was observed to decrease with increasing magnification. This decrease agreed with Eq. (5), given by Clemens.[18] Despite this loss of signal and considering that the fluorescence of OH is relatively intense, the 203.2 mm extension tube configuration was chosen in order to maximize the planar resolution of the PLIF images. Figure 6 compares theoretical and measured values for magnification, image intensity, and resolution limit at different extention tube lengths.

$$RL \cdot M = 77 \ \mu m \qquad (4)$$

$$I \propto (M + 1)^{-2} \qquad (5)$$

The camera was focused on a 1 mm grid dotcard which was illuminated at a very shallow angle by the laser sheet. An analysis of the dotcard images indicated a square field of view $6.86 \times 6.86$ mm across $512 \times 512$ pixels (using $2 \times 2$ binning of the $1064 \times 1064$ pixel array). Pixel binning was used to increase the signal-to-noise ratio. The system therefore had 76.8 pixels/mm or 13.4 μm per binned pixel. The sensor for the PI-Max 4 is $13.1 \times 13.1$ mm; therefore $M = 1.91$. Through Eq. (4), expected in-plane resolution for PLIF images was 40 μm.
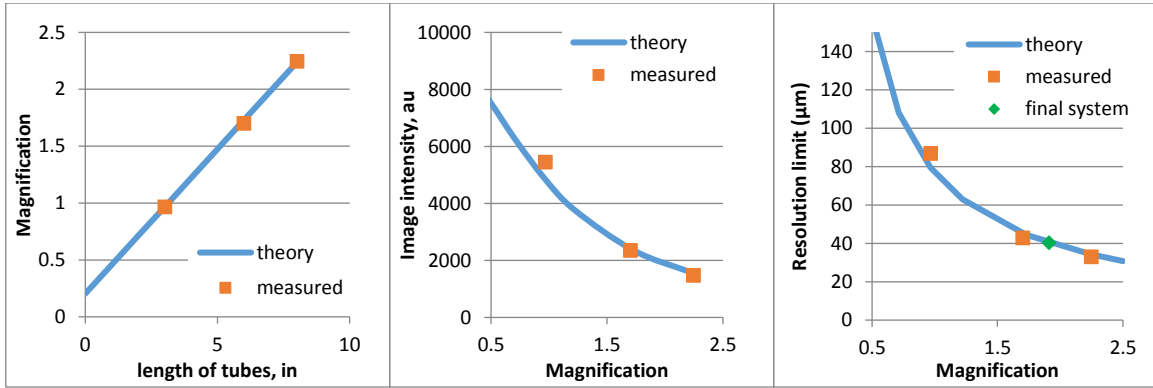


**Figure 6. Comparisons between extension tube length, magnification, image intensity, and resolution limits.**

## III.     Experimental procedures

Three test cases were investigated (Table 1.) Case A represents the standard test conditions for the facility. Cases B and C have reduced fuel/air equivalence ratio and total temperature, respectively. These cases represent conditions near blow off. The facility air throttle was not used for any test case. After establishing the Case A flame in the facility, the laser sheet was directed onto the spanwise centerline. The camera was then focused on the fluorescence produced by the excitation of the flame by the laser sheet. The camera was set to record images at 75% of maximum gain, with a gate duration of 150 ns. The camera was triggered by the Nd:YAG laser. Due to bandwidth limits, the camera acquired images at 10 Hz, with every second laser pulse.

|  | Case A (base) | Case B (low-$\phi$) | Case C (low-$T_0$) |
|---|---|---|---|
| $T_0$ (K) | 1200 | 1200 | 1100 |
| $P_0$ (kPa) | 300 | 300 | 300 |
| $\phi_{cavity\ wall}$ | 0.21 | 0.17 | 0.21 |
| $\phi_{observation\ wall}$ | 0.20 | 0.17 | 0.21 |
| $M_{combustor}{}^{9}$ | 0.73 | 0.73 | 0.73 |

**Table 1. UVaSCF test conditions**

Images were taken while the translation system's $x$-axis motor was in motion. The camera travelled along the $x$-axis at 0.25 mm/s while acquiring images at 10 Hz, resulting in 40 images taken for every millimeter travelled. Six $x$-direction sweeps were acquired from $x/H = 0$ to 14.10, and from $y/H = $ -0.67 to 2.70 for cases A and B. Case C data was confined to a smaller range, due to fuel limitations. Most $(x,y)$ point locations were measured 275 times. Regions

of overlap between scans received more measurements. Regions near the start or the end of each scan received fewer measurements during the scans; however, where these reduced-coverage regions occurred near the cavity flameholder, extra images were acquired with the camera stationary. Approximately 15,000 images were captured for each case. A sweep of background images was taken at a speed of 1 mm/s, over the same *x* range and at *y/H* = -0.11. These images were taken with combustion active, but with the laser blocked.

Occasionally, it was necessary to refocus the camera. This may have been caused by gradual heating and expansion of the facility, camera support structure, and lens tube. The camera was focused based on the observed sharpness of flame structures. Focusing motions were very small, because the depth of focus of the camera was on the order of one millimeter.

# IV.    Results

## A. Flame statistics

MATLAB scripts were developed to compute statistics from the acquired PLIF images. Each pixel in each background image was assigned an *x*-coordinate, and mean background counts as a function of *x*-position was computed. This background intensity function was used to subtract a background signal level from the instantaneous images and mean image data shown below. Each pixel in each PLIF image was assigned *x*- and *y*-coordinates. These coordinates were used to map data from each image onto a $2312 \times 9473$ pixel matrix spanning the entire observed region. A compilation of single images from Case A are displayed in Fig. 7. Mean intensity (Fig. 8) was calculated for each pixel location in the matrix.
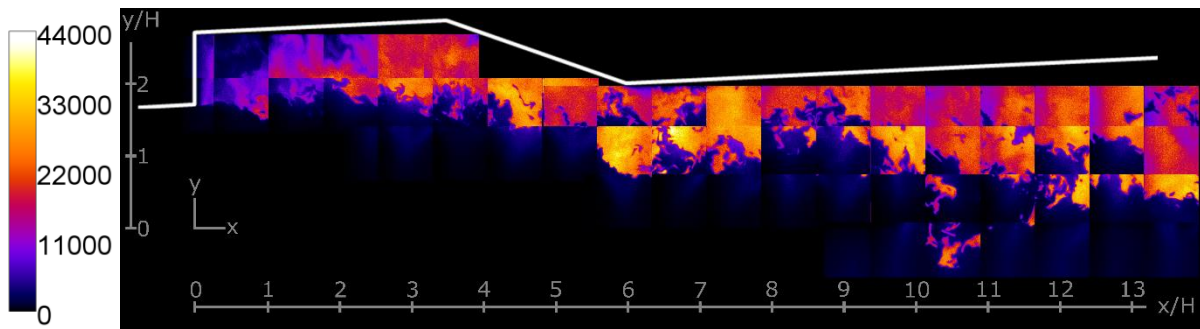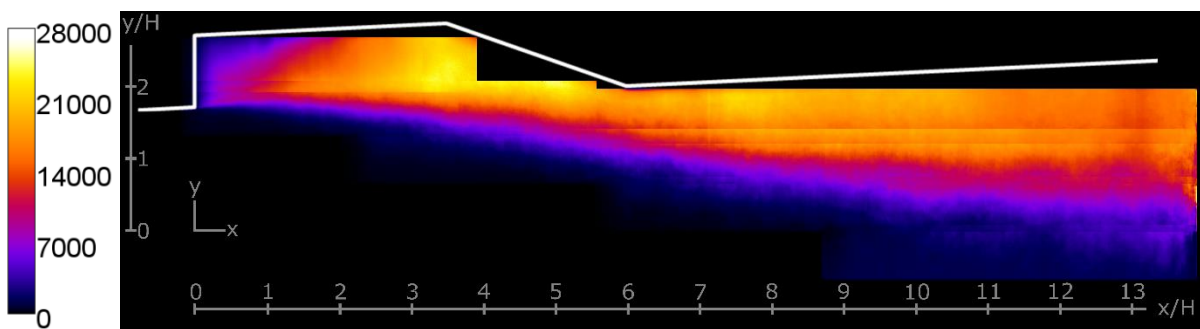


**Figure 7. OH PLIF single-image compilation, Case A.**



**Figure 8. Mean OH PLIF signal intensity, Case A.**

Flame intermittency[19,20] was calculated to provide a statistical measurement of flame front movement. For each pixel location, intermittency is defined[1] as the proportion of images in which the OH signal is above a specified threshold. A threshold of 6,000 counts was used to binarize all images into bright regions, indicating significant concentrations of OH and other reactants, and dark regions, indicating a lack of significant OH concentration. The thresholded images were averaged across a $2312 \times 9473$ pixel matrix and converted to a percentile scale, creating an intermittency image. This image was thresholded to create contours of 5%, 50%, and 95% intermittency, displayed in Fig. 9. These contours provide a visualization of the spatial envelope in which the flame oscillates.
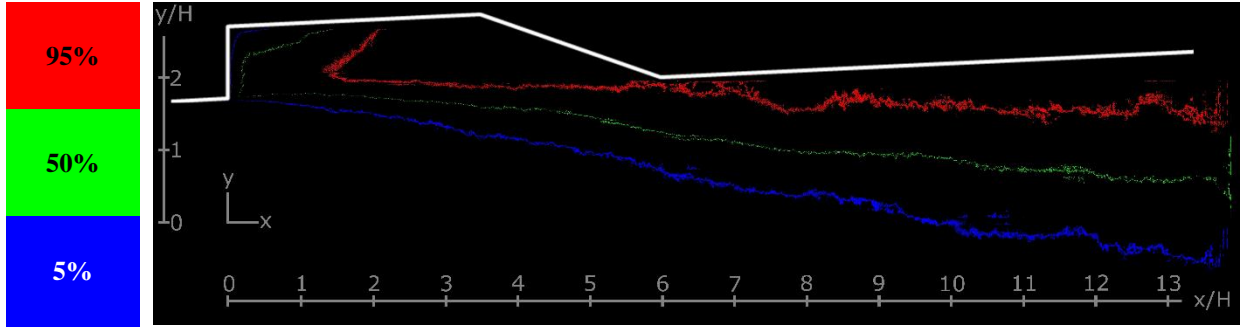
**Figure 9. Intermittency contours, Case A.**

Intermittency was also used to calculate flame angles and compare different test conditions. The flame angle is the angle between the free stream (the *x*-direction) and the line traced by the outer boundary of the flame. Intermittency data from all three cases was thresholded to create 5% contours. Intermittency contours include a small region near the backward-facing step that does not follow the flame front; these pixels were ignored. Figure 10 displays the resulting 5% intermittency contours.

|  | Case A (base) | Case B (low-$\phi$) | Case C (low-$T_0$) |
|---|---|---|---|
| Current work | 9.8° | 10.3° | 7.73° |
| Cantu et. al. [1] | 10.4° | 11.1° | |

**Table 2. Flame angle comparisons based on 5% intermittency**

A line of best fit was plotted through each contour; this line defined the flame angle. Table 2 lists the flame angles for the three cases and compares them with data obtained at lower resolution by Cantu et. al.[1] It is important to note that the study by Cantu et. al. calculated intermittency using a threshold at 20% of the maximum signal for each image, binarizing each image differently. The smaller field-of-view in the current work creates many low-contrast images in which the flame front is not present. A percentile threshold does not binarize these images appropriately, so a constant threshold was chosen; this complicates comparison with Cantu et. al.

Flame angles for Cases A and B are smaller than the values from the previous work by less than one degree. An increase in flame angle with decreased $\phi$ was noted in both experiments. In the current work, flame angle decreased with decreased $T_0$. No comparison with Case C in the current work was possible, because the low-$T_0$ case in the previous work was conducted with the air throttle on.
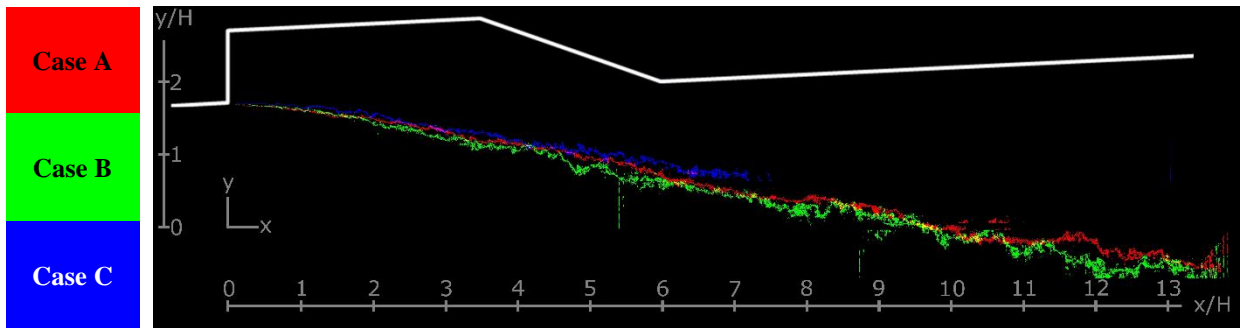


**Figure 10. 5% intermittency contours for three test cases.**

## B. Single image analysis

Single OH PLIF images provide instantaneous measurements of the shape of the flame at different points in the flow. The relevant flame timescales are too short to capture with 10 Hz imaging, so the images have no temporal correlation. OH signal denotes areas of products of combustion; lack of signal implies the presence of reactants. The three single images in Figure 11 show different levels of turbulence based on the size of flow structures imaged, from least turbulent at the left to most turbulent at the right. All single images presented in this section are from Case A, in the shear layer adjacent to the cavity. The leftmost image shows a flame front that is wrinkled but connected throughout, which is typical of images acquired at this spatial location. The other two images, obtained further downstream, show increasingly wrinkled flames and distributed flame regions.
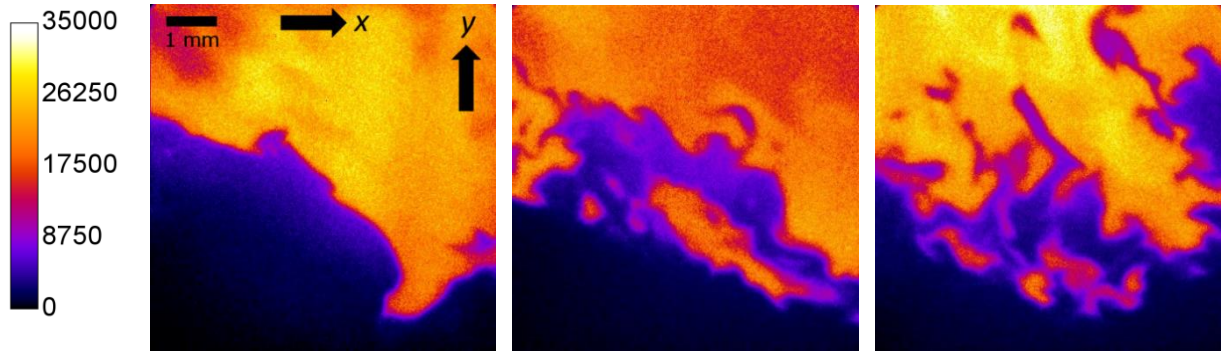
**Figure 11. Single OH PLIF images.** *Image center coordinates, left to right: x/H = 1.88, 2.42, 4.09, y/H = 1.71.*

Images were searched manually for very thin OH structures. One such structure is shown in Fig. 12. The length of this structure is representative of the smallest structures observed. An intensity profile (Fig. 13) was calculated across the structure at the location of the yellow line. The Gaussian fit for the profile had FWHM = 110 µm. This is somewhat greater than the minimum structure size prediction ($10\eta \approx 70$ µm.) No structures close in size to the expected resolution limit of the system (40 µm) were observed. This suggests that this OH PLIF system is able to resolve the smallest features of the flow. Further investigations of the data will compare flame structures in the vicinity of the cavity with those further downstream.
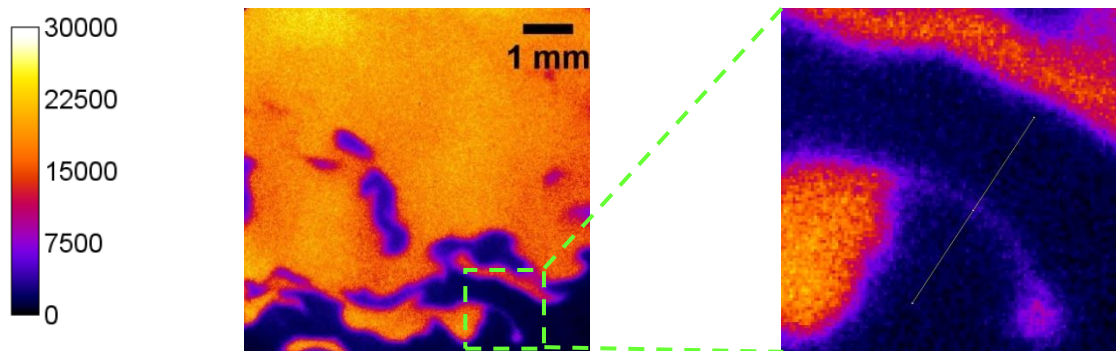


**Figure 12. Small flame structure.** *Full image center coordinates: x/H = 5.60, y/H=1.60.*
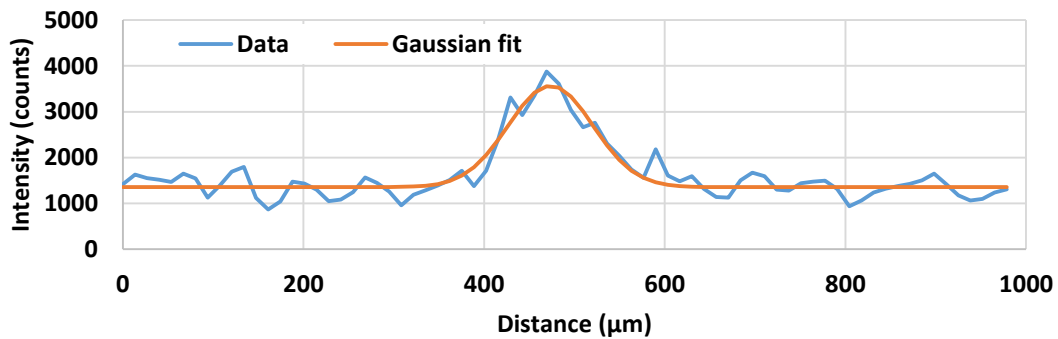


**Figure 13. Intensity profile of small flame structure.**

## C. Turbulence analysis

A simple, automated method was used to calculate the local flame surface density in OH PLIF images. Flame surface density *FSD* is the surface area of the flame per unit volume;[21] this serves as a metric for the level of turbulence of a flame. In this work, *FSD* is calculated for each single image as a local quantity that varies with position. The *FSD* is analogous to the length of the path that the flame front takes through an image; it describes the extent to which the flame in the field-of-view is wrinkled. The border of a region of high OH signal corresponds to the boundary between reactants and products; it is a rough measure of the location of the flame front.[22] The flame front for a perfectly

laminar flame would trace a straight line across the image; as *FSD* increases, the flame front turns and traces a longer path throught the image, sometimes forming separated islands.

All images were processed using the application ImageJ. First, the images were thresholded and converted to binary. Thresholding was conducted using the ImageJ "default" method, based on an iterative selection method.[23] This method binarized each image differently, as opposed to the constant threshold described in Section IV. A. No constant threshold was observed to binarize pixels near the flame front appropriately for all images. Thresholding set pixel intensities *I* to one (bright) or zero (dark.) Outliers of radius three pixels and smaller were removed (bright outliers first, then dark.) The magnitude of the gradient (using pixel coordinates $x_p$ and $y_p$ from 0 to 512) of the image was calculated, and the mean of all pixel values in the gradient image was defined as the local *FSD* for the corresponding OH PLIF image. Equation (6) describes this calculation; this process for calculating *FSD* is similar to that of Hult et. al.[21]

$$FSD = \left\langle \sqrt{\left(\partial I / \partial x_p\right)^2 + \left(\partial I / \partial y_p\right)^2} \right\rangle \tag{6}$$

For images that contain large areas of high signal and low signal, this threshold/gradient process produces a well-defined trace of the flame front, though very small features are often lost. Figure 14 shows each of these steps for such an image. The process fails for images without large distinct contrasting regions. The threshold does not capture the flame front (because little to none of the flame front is present in the image) and draws a meaningless, blurred contour instead. This leads to non-physical, abnormally high values of *FSD*. Such a failure is shown in Fig. 15.



**Figure 14. Threshold/gradient process success.** $FSD = 2.134 \times 10^{-2}$.
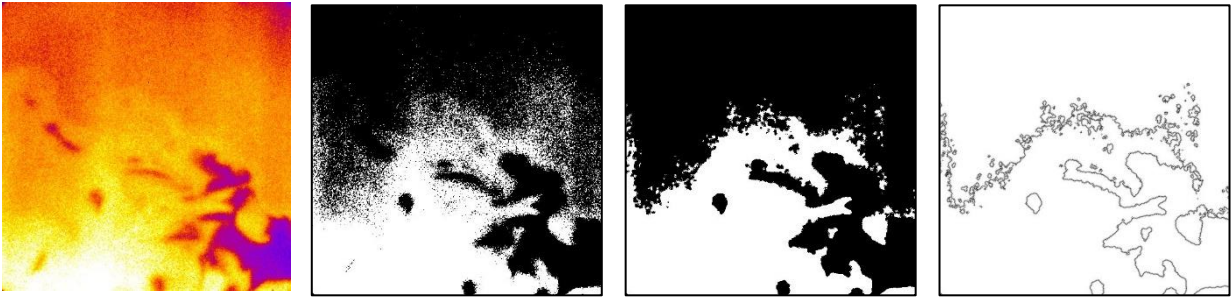


**Figure 15. Threshold/gradient process failure.** $FSD = 4.170 \times 10^{-2}$.

Figure 16 shows the images from Fig. 11 after implementing the threshold/gradient process. The *FSD* values for these images follow the trend expected from a visual analysis of turbulence. By calculating average *FSD* values at different *(x,y)* locations, we may draw conclusions about the effect of position on flame structure. Figure 17 shows mean *FSD* values for three scans across the test section for Case A, with the 48-52% intermittency contour superimposed. It is important to note that this data includes process failures – very high *FSD* values occur when the intermittency is not close to 50%. *FSD* data should be discounted in regions away from 50% intermittency, such as the two regions of very high *FSD* in Fig. 17. The data shows a general trend towards higher *FSD* as the flow proceeds downstream. This method could be applied to computational investigations of the flame for direct comparison with experimental results.
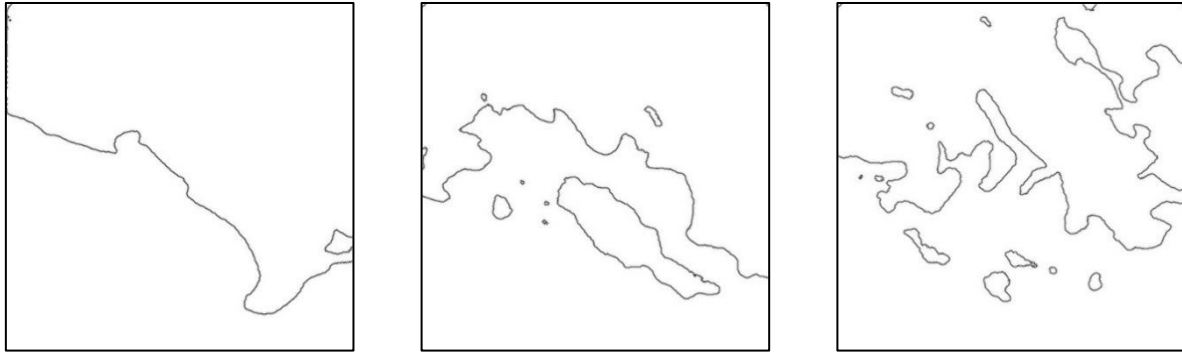
**Figure 16. Threshold/gradient images.** *Left to right, FSD = $6.910 \times 10^{-3}$, $1.367 \times 10^{-2}$, $2.273 \times 10^{-2}$.*
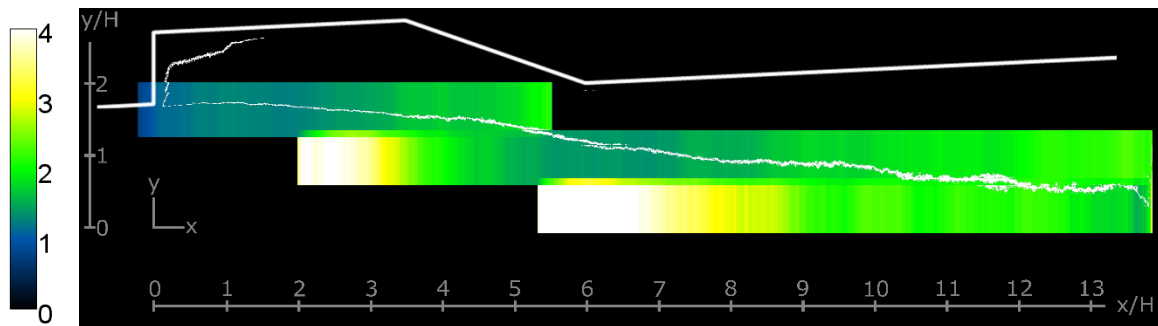


**Figure 17. Plot of flame surface density $\times 10^{-2}$, Case A.**

## V.    Conclusions

A high-spatial-resolution OH PLIF system was constructed to image fine structures in a premixed turbulent compressible reacting flow.  The system has an spatial resolution limit of $40 \times 40 \times 25$ μm.  The system was used to image a flame anchored by a cavity flameholder with a backward-facing step of height 9 mm. Standard test conditions comprised $T_0 = 1200$ K, $p_0 = 300$kPa, $\phi_{combustor} \approx 0.4$ and $M_{combustor} \approx 0.73$. The flame was also imaged at a low-$T_0$ case and a low-$\phi$. Flame angle was measured for all three cases.  Relative to standard conditions, the low-$T_0$ flame angle was larger and the low-$\phi$ flame angle was smaller. Signal intensity statistics were computed for the observed area. The smallest observed features in the flow were approximately 110 μm wide.  An automated method was developed to calculate local flame surface density in OH images.  This method indicated an increase in flame surface density as the flow moves downstream.  This study has provided a large quantity of data that will be compared with computational results in order to refine computational and analytical models of turbulent combustion.

## Acknowledgements

## References

[1] Cantu, L. M. L., Gallo, E. C. A., Cutler, A. D., Danehy, P. M., Rockwell, R. D., Johansen, C. T., Goyne, C. P., and McDaniel, J. C.. "OH PLIF Visualization of a Premixed Ethylene-fueled Dual-Mode Scramjet Combustor," *54th AIAA Aerospace Sciences Meeting, AIAA SciTech Forum*, AIAA, 2016.

[2] Kychakoff, G., Howe, R. D., Hanson, R. K., McDaniel J. C., "Quantitative visualization of combustion species in a plane," *Applied Optics*, Vol. 21, No. 18, 1980, pp. 3225-3227.

[3] Boxx, I., Arndt, C. M., Carter, C. D., Meier, W., "High-speed laser diagnostics for the study of flame dynamics in a lean premixed gas turbine model combustor," *Experiments in Fluids*, Vol. 52, No. 3, 2012, pp. 555-567.

[4] Gabet, K. N., Patton, R. A., Jiang, N., Lempert, W. R., Sutton, J. A.. "High-speed $CH_2O$ PLIF imaging in turbulent flames using a pulse-burst laser system," *Applied Physics B*, Vol. 106, 2012, pp. 569–575

[5] Boeckle, S., Kazenwadel, J., Kunzelmann, T., Shin, D., Schulz, C., Wolfrum, J.. "Simultaneous single-shot laser-based imaging of formaldehyde, OH, and temperature in turbulent flames," *Proceedings of the Combustion Institute*, Vol. 28, 2000, pp. 279–286.

[6] Ayoola, B. O., Balachandran, R., Frank, J. H., Mastorakos, E., Kaminski, C. F., "Spatially resolved heat release rate measurements in turbulent premixed flames," *Combustion and Flame*, Vol. 144, 2006, pp. 1-16.

[7] Krauss, R., and McDaniel, J. C., "A clean air continuous flow propulsion facility," *28th Joint Propulsion Conference and Exhibit, Joint Propulsion Conferences*, AIAA, 1992.

[8] Rockwell, R. D., Goyne, C. T., Haw, W., Krauss, R., McDaniel, J. C., and Trefny, C., "Experimental Study of Test Medium Vitiation Effects on Dual-Mode Scramjet Mode Transition," *48th AIAA Aerospace Sciences Meeting Including the New Horizons Forum and Aerospace Exposition, Aerospace Sciences Meetings*, AIAA, 2010.

[9] Rockwell, R. D., Goyne, C. P., Rice, B., Chelliah, H. K., McDaniel, J. C., Edwards, J. R., Cantu, L. M. L., Gallo, E. C. A., Cutler, A. D., Danehy, P. M., "Development of a Premixed Combustion Capability for Dual-Mode Scramjet Experiments," *53rd AIAA Aerospace Sciences Meeting, AIAA SciTech Forum*, AIAA, 2015.

[10] Filatyev, S. A., Driscoll, J. F., Carter, C. D., Donbar, J. M., "Measured properties of turbulent premixed flames for model assessment, including burning velocities, stretch rates, and surface densities," *Combustion and Flame*, Vol. 141, No. 1, 2005, pp. 1-21.

[11] Tennekes, H., and Lumley, J. L., "Length scales in turbulent flows," *A First Course in Turbulence*, 2nd ed., MIT Press, Cambridge, 1973, pp. 14-24.

[12] Ramesh, K., Edwards, J. R., Goyne, C. P., McDaniel, J. C., Cutler, A. D., Danehy, P. M., "Large Eddy Simulation of High-Speed, Premixed Ethylene Combustion," *53rd AIAA Aerospace Sciences Meeting*, AIAA, 2015.

[13] Westerweel, J., Elsinga, G. E., Adrian, R. J., "Particle Image Velocimetry for Complex and Turbulent Flows," *Annual Review of Fluid Mechanics*, Vol. 45, 2013, 409-436.

[14] Driscoll, J. F., "Turbulent premixed combustion: Flamelet structure and its effect on turbulent burning velocities," *Energy and Combustion Science*, Vol 34, 2008, pp. 91-134.

[15] Kobayashi, H., Kawahata, T., Seyama, K., Fujimari, T., Kim, J., "Relationship between the smallest scale of flame wrinkles and turbulence characteristics of high-pressure, high-temperature turbulent premixed flames," *Proceedings of the Combustion Institute,* Vol. 29, No. 2, 2002, pp. 1793-1800.

[16] O'Byrne, S., Stotz, I., Neely, A., Boyce, R., Mudford, N., and Houwing, F., "OH PLIF Imaging of Supersonic Combustion Using Cavity Injection," *AIAA/CIRA 13th International Space Planes and Hypersonics Systems and Technologies Conference, International Space Planes and Hypersonic Systems and Technologies Conferences*, AIAA/CIRA, 2005

[17] Smith, W. J., "The Modulation Transfer Function," *Modern optical engineering: the design of optical systems*, New York: McGraw Hill, 2000, pp. 366–372.

[18] Clemens, N. T., Hornak, J. P. (Ed.) 2002. "Flow Imaging," *Encyclopedia of Imaging Science and Technology*. New York: Wiley, 2002, pp. 390-419.

[19] Cheng, R. K., Shepherd, I. G., "Intermittency and Conditional Velocities in Premixed Conical Turbulent Flames," *Combustion Science and Technology*, Vol. 52, No. 4-6, 1987, pp. 353-375.

[20] Tennekes, H., and Lumley, J. L., "Turbulent wakes," *A First Course in Turbulence*, 2nd ed., MIT Press, Cambridge, 1973, pp. 113-124.

[21] Hult, J., Gashi, S., Chakraborty, N., Klein, M., Jenkins, K. W., Cant, S., Kaminski, C. F., "Measurement of flame surface density for turbulent premixed flames using PLIF and DNS," *Proceedings of the Combustion Institute*, Vol. 31, 2007, pp. 1319-1326.

[22] Paul, P. H., Najm, H. N., "Planar Laser-Induced Fluorescence Imaging of Flame Heat Release Rate," *Symposium (International) on Combustion*, Vol. 27, 1998, pp. 43-50.

[23] Ridler, T. W., Calvard, S., "Picture thresholding using an iterative selection method," *IEEE Transactions on Systems, Man, and Cybernetics*, Vol. 8, 1978, pp. 630-632.